iScience

CellPress
OPEN ACCESS

Article

Modifying MSCs-derived EVs with esterase-responsive and charge-reversal cationic polymers enhances bone regeneration

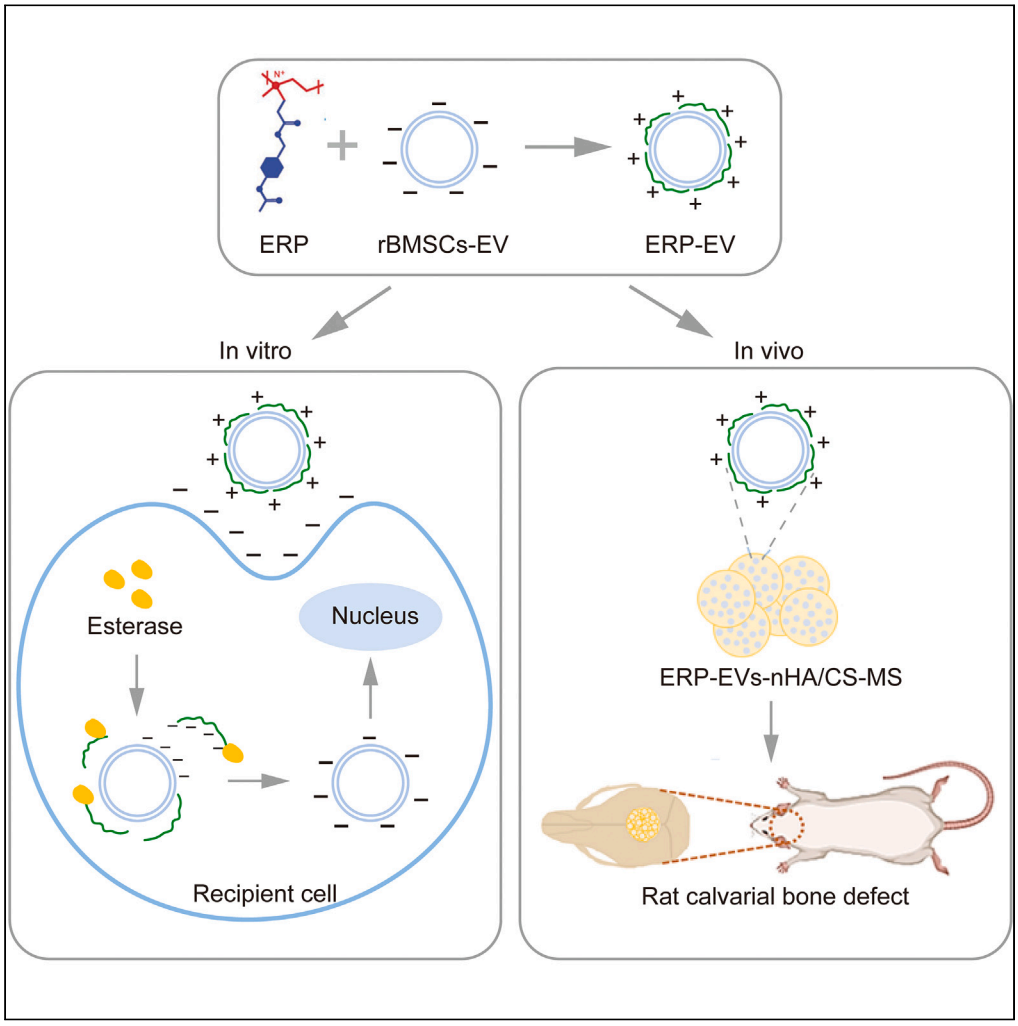

Yihan Chen, Bang Li, Mukeshimana Christelle, ..., Nasha Qiu, Hengguo Zhang, Jianguang Xu

hzhou@ahmu.edu.cn (H.Z.)
qiunasha@163.com (N.Q.)
zhanghengguo@ahmu.edu.cn (H.Z.)
xujianguang@ahmu.edu.cn (J.X.)

Highlights

ERP-EVs significantly increased the uptake efficiency by BMSCs

ERP-EVs promoted the osteogenic differentiation of BMSCs *in vitro*

ERP-EVs were uptaken more by BMSCs than other bone-related cells

ERP-EVs-nHA/CS-MS promoted the new bone formation *in vivo*

Chen et al., iScience 27, 110801
September 20, 2024
https://doi.org/10.1016/j.isci.2024.110801

iScience

CellPress
OPEN ACCESS

Article

Modifying MSCs-derived EVs with esterase-responsive and charge-reversal cationic polymers enhances bone regeneration

Yihan Chen,[1,2,5] Bang Li,[1,5] Mukeshimana Christelle,[1] Nshimiyimana Eugene,[1] Wenjia Han,[1] Hong Zhou,[3,*] Nasha Qiu,[4,*] Hengguo Zhang,[1,*] and Jianguang Xu[1,6,*]

SUMMARY

Extracellular vesicles (EVs) derived from mesenchymal stem cells (MSCs) for the treatment of bone defects have been widely reported as a cell-free therapy because of their appropriate stability and biocompatibility. However, EV isolation is expensive and time-consuming. We developed a method of modifying EVs derived from bone marrow MSCs (BMSCs) via the cationic polymer (ERP) with characteristics of charge reversal and esterase response (ERP-EVs). When simply mixing BMSCs-EVs with ERP at a 1:1 ratio, ERP-EVs significantly enhanced the osteogenesis of BMSCs. More EVs were released by ERP in BMSCs than in fibroblasts, realizing the selective release. Last, ERP-EVs were loaded on an nHA/CS-MS scaffold and showed enhanced bone regeneration on rat calvarial bone defects *in vivo*. In general, this study provided an effective strategy to improve cellular uptake and selective release of BMSCs-EVs in bone-related cells, which had great potential to accelerate the clinical practice of BMSCs-EVs-based bone defect repair.

INTRODUCTION

The alveolar bone defect is among the most common complications that compromise maxillofacial functions. The defect can result from injury, infections, tumors, or cysts.[1] Bone substitution materials that mimic the bone tissue features are used to repair alveolar bone defects.[2] Besides, mesenchymal stem cells (MSCs) therapy has emerged due to its capacity to promote bone regeneration and its immunomodulatory potential. However, clinical translation of MSCs still has some limitations such as high cellular heterogeneity and certain safety concerns.[3]

MSCs-derived extracellular vesicles (EVs), which are of great importance in cell communication, have been regarded as a substitute for MSCs in the treatment of bone defects.[4] EVs are packaged by lipid bilayers, whose diameters are around 40–120 nm. They carry various elements secreted by parent cells, involving DNA, mRNA, lipids, and proteins.[5] EVs are taken up by recipient cells mainly through endocytosis and membrane fusion to accomplish cellular communication.[6] Because of their superior stability and biocompatibility to stem cells, EVs have been utilized as a "cell-free therapy" in bone regeneration.[7] However, isolation and extraction of EVs from MSCs are time-consuming, which is a tough issue for clinical translation. Meanwhile, the low uptake efficiency and non-specific uptake by recipient cells may sharpen this problem.

Recently, various methods have been utilized to modify EVs, including covalent modification, non-covalent modification, active loading, etc.[7] For example, Sato et al. improved the half-life period of EVs by combining them with liposomes via a freeze-thaw method.[8] Tian et al. significantly optimized the target specialty of lesion region of cerebral ischemia through engineered c(RGDyK)-conjugated EVs.[9] Zhang et al. produced engineered EVs by electroporation which induced vascularized osteogenesis.[10]

It is suggested that MSCs-EVs modified with cationic polymers could achieve efficient uptake of recipient cells without damaging the integrity and function of EVs and improve their uptake efficiency to recipient cells. Commonly, cationic polymers combine negatively charged nucleic acid molecules to form positively charged nanocomplexes. Previous studies have successfully combined negatively charged EVs with biomaterials involving cationic polymer adsorption (such as PEI) and cationic liposomes.[8,11]

Enhancement of cell targeting specificity of EVs is another goal through EVs modification. Esterase is an endogenous, hydrolase that widely exists in the cytoplasm and nucleus.[12] By introducing the chemical bonds sensitive to esterase, such as ester bonds, into the cationic polymer, the polymer could be hydrolyzed to form negative carboxylic acid under the reaction of intracellular esterase, thereby reducing the electrostatic binding force between the polymer and delivery cargos.[13] Previous study certificated that bone marrow displays a high level of esterase activity when compared to other tissues.[14] Bone marrow MSCs (BMSCs) and macrophages, which play a critical role in bone defect

[1]College & Hospital of Stomatology, Anhui Medical University, Key Lab. of Oral Diseases Research of Anhui Province, Anhui, China
[2]Restorative Dental Sciences, Endodontics, Faculty of Dentistry, The University of Hong Kong, Hong Kong, SAR, P.R. China
[3]Department of Cell and Biology, College of Life Sciences, Anhui Medical University, Anhui, China
[4]The Center for Integrated Oncology and Precision Medicine, Key Laboratory of Integrated Oncology and Intelligent Medicine of Zhejiang Province, Hangzhou First People's Hospital, Hangzhou, China
[5]These authors contributed equally
[6]Lead contact
*Correspondence: hzhou@ahmu.edu.cn (H.Z.), qiunasha@163.com (N.Q.), zhanghengguo@ahmu.edu.cn (H.Z.), xujianguang@ahmu.edu.cn (J.X.)
https://doi.org/10.1016/j.isci.2024.110801

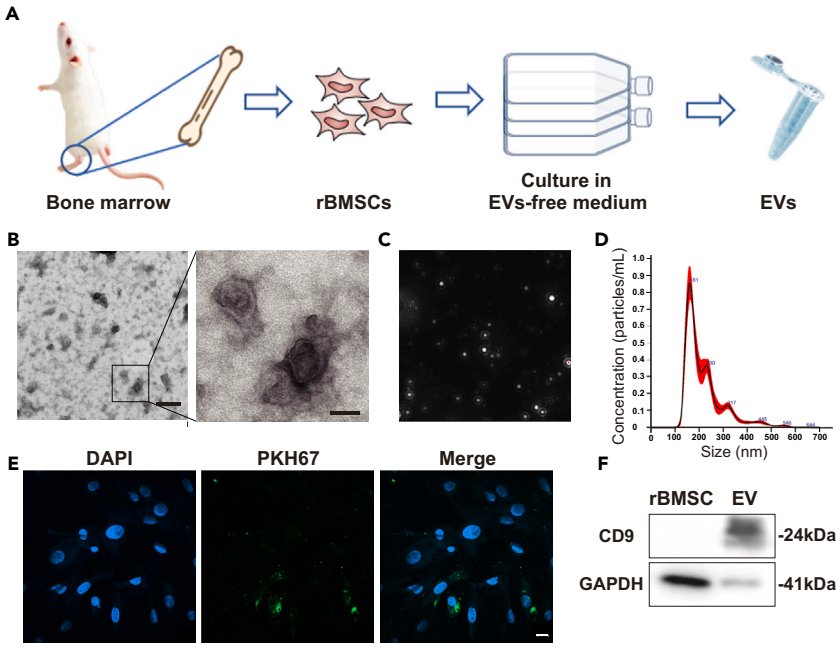

Figure 1. Identification of rBMSCs-EVs

(A) Illustration of the extraction protocol.

(B) Morphology of rBMSC-EVs under a TEM. The scale bar in the left figure represents 200 nm. The scale bar in the right figure represents 50 nm.

(C and D) Image and particle size of rBMSCs-EV particles detected by NTA.

(E) Confocal images of cellular uptake of PKH67-labeled rBMSCs-EVs by rBMSCs, scale bar, 20 μm.

(F) Western blot analysis of CD9 expression in rBMSC and EV.

repair, showed a higher intracellular esterase level than other cells such as fibroblast-like cells.[15,16] Thus, the selective release of BMSCs-EVs in different recipient cells during bone regeneration is a potential strategy for weakening the effect on other irrelevant cells.

Here, we introduced an esterase-responsive charge-reversal cationic polymer (N-[3-(*p*-acetyloxybenzyloxyoxo) propyl)]-N-methyl-quaternized PEI, simply called ERP), which is also based on intracellular esterase response.[13] We modified EVs with ERP. After ERP-EVs are internalized by recipient cells, intracellular esterase will trigger ERP hydrolyzation to reverse its charge, promoting EVs to release from ERP and promote osteogenesis of recipient cells. Finally, we uploaded ERP-EVs into hydroxyapatite/chitosan-microspheres (HA/CS-MS),[17] a scaffold matrix that provides structural support for new bone tissue ingrowth, to enhance *in vivo* new bone formation.

RESULTS

Identification of rBMSCs-EVs

EVs derived from rBMSCs were isolated by ultracentrifugation (Figure 1A). The morphology of rBMSCs-EVs observed by Transmission Electron Microscopy (TEM) was round-like, with a dark circle surrounding it, which was considered to be the lipid bilayer (Figure 1B). The rBMSCs-EV particles were evenly distributed in PBS with proper concentration and visual field when being texted (Figure 1C). The result of Nanoparticle Tracking Analysis (NTA) indicated the heterogeneity of rBMSCs-EVs. The diameter peak of rBMSCs-EV was at 161 nm. Some of them were larger than 230 nm (Figure 1D). CD9 is a membrane surface marker of EVs. The result of western blot showed that rBMSCs-EVs expressed CD9 whereas rBMSCs lacked the corresponding marker (Figure 1F). When co-cultured rBMSCs with rBMSCs-EVs after 4 h at the concentration of 1×10^6 particles/mL, we demonstrated that rBMSCs-EVs could be internalized by rBMSCs. However, the amount of rBMSCs-EVs absorbed by rBMSCs differed between each cell. The green fluorescence was evident in certain rBMSCs while others barely showed EVs uptake (Figure 1E).

ERP reversed the surface charge of rBMSCs-EV

ERP was a modified cationic polymer carrying a positive charge (Figures 2B and 2G), whereas rBMSCs-EV had a negative charge surface (Figure 2G). Firstly, we demonstrated that the average diameter of ERP was 32.1267 ± 0.3553 nm (Figure 2A). Then we assessed the effect of ERP on cell survival and proliferation. No significant difference was found when the concentration of ERP was no higher than 50 μg/mL, but ERP showed significant cytotoxicity when the concentration was more than 100 μg/mL (Figure 2C). The result indicated that the appropriate dosage for further co-culture system using ERP should be no higher than 50 μg/mL. After that, we mixed ERP with rBMSCs-EV in PBS and co-cultured them with rBMSCs in 4 h and 24 h. We confirmed that ERP-EVs significantly promoted cell proliferation (Figure 2D). However, ERP-EV still showed acceptable cytotoxicity compared with the EVs sample group in the early stage.

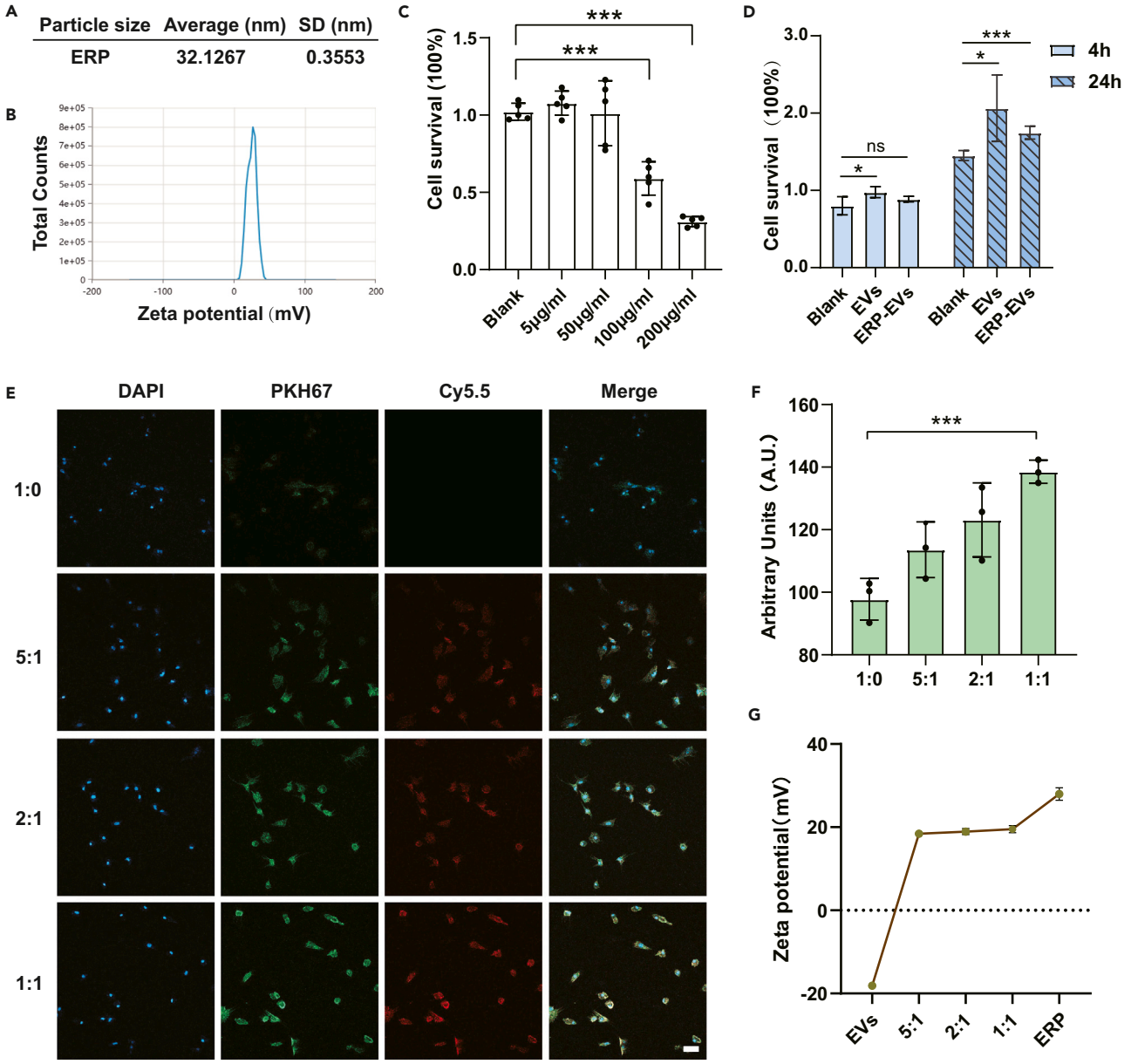

Figure 2. EVs modified with ERP

(A and B) Particle size and Zeta potential of ERP measured by DLS.

(C) Cytotoxicity of ERP on rBMSCs as evaluated by CCK8 assay.

(D) Cell viability of rBMSCs when co-cultured with EVs and a 1:1 mixture of ERP-EVs using CCK-8 assay.

(E) The uptake efficiency of rBMSCs to ERP-rBMSCs-EVs at different microparticle ratios observed by CLSM. Scale bar, 50 μm.

(F) The quantity measurement of mean fluorescence strength by ImageJ.

(G) Zeta potential of rBMSCs-EVs and ERP-rBMSCs-EVs incubated with different microparticle ratios. Data are presented as mean ± SEM. Differences in expression between groups were calculated by one-way ANOVA. (*$p < 0.05$, **$p < 0.01$, ***$p < 0.001$).

We hypothesized that simply mixing ERP and EVs in PBS would make them combine and reverse the surface electric charge of rBMSCs-EVs. We marked rBMSCs-EVs and ERP with PKH67 and Cy5.5, respectively. The overlap of two fluorescence was observed, which demonstrated the successful combination of ERP-EV (Figure 2E). We set different ratios of the proportion of ERP and EV (EV: ERP = 1:0, 5:1, 2:1, 1:1) to assess which ratio could achieve charge reversal. The result indicated that the surface electric charge of EVs was reversed to a positive charge once ERP was added. Zeta potential was maintained at +20 mV (Figure 2G). Also, the diameter of ERP-EVs combined with different ratios was conducted via NTA assessment. The result demonstrated that the size of ERP-EVs with different ratios increased approximately 2-fold than pure EVs (Figure S1). Namely, the particle size of ERP-EVs with different ratios were 312.2 ± 70.8 nm (5:1),

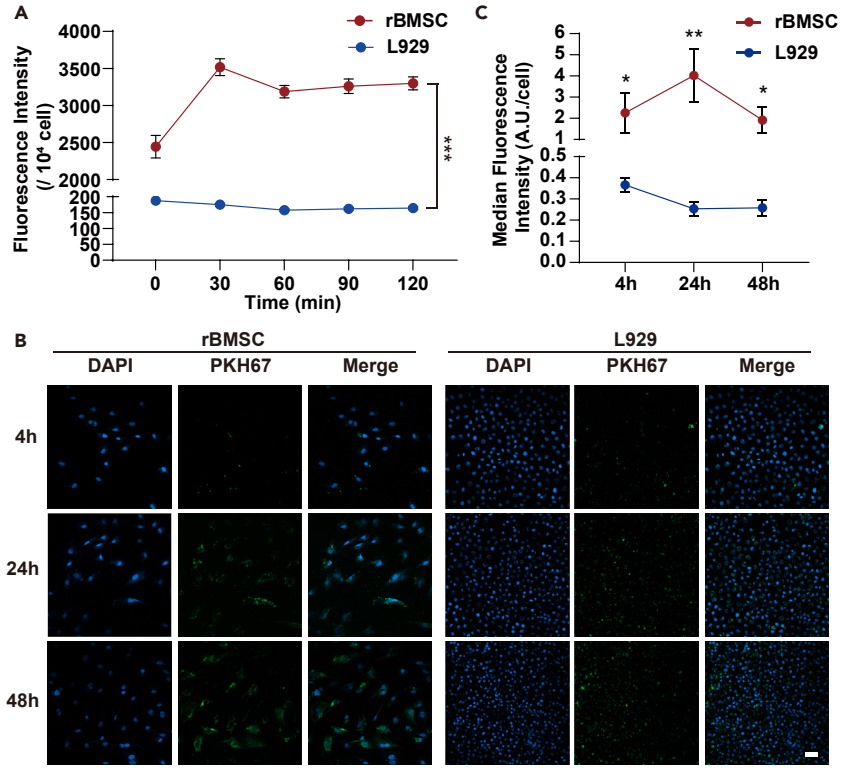

Figure 3. EVs were efficiently released from ERP via esterase-hydrolyzation

(A) rBMSCs and L929 were treated with FDA to measure the content of cellular esterase levels.

(B and C) Cellular uptake efficiency at different time points observed by inverted fluorescent microscope and their median fluorescence intensity. Data are presented as mean ± SEM. Differences in expression between groups were calculated by t test. (*$p < 0.05$, **$p < 0.01$, ***$p < 0.001$).

326.8 ± 69.4 nm (2:1), and 346 ± 63.1 nm (1:1), respectively. With more ERP added to incubation, the size increased and reached the maximum when the combination ratio was 1:1.

To optimize the ratio of ERP-EVs for further experiments, we assumed that the highest uptake efficiency was most suitable for the functionality of rBMSCs. A confocal fluorescence microscope was used to assess the uptake efficiency of ERP-EVs. The result showed that the green fluorescence became stronger than the EVs sample group with an increased ERP ratio (Figure 2E). To quantify the influence of different ratios on the uptake of rBMSCs, we measured fluorescence strength by ImageJ. The mean fluorescence strength was significantly increased when the ratio was 1:1. Additionally, TEM indicated that ERP particles covered approximately half of the surface of EVs when the combination ratio reached 1:1 (Figure S2). Altogether, we used a 1:1 ratio for further assessment.

EVs were efficiently released from ERP via esterase-hydrolyzation

ERP was not only a cationic polymer but also had the characteristic of esterase response. We analyzed the content of esterase in rBMSCs and L929, concluding that rBMSCs were far more abundant in cellular esterase than L929 (Figure 3A). The same amount of ERP-EVs was added to two cell types, respectively. Different time points (4 h, 24 h, 48 h) were set to measure the uptake efficiency. After 24 h of co-culture, we replaced fresh media without ERP-EV to analyze whether EVs play a role inside the cells. The result demonstrated that the mean uptake efficiency by rBMSCs was significantly higher than L929. Meanwhile, the reduction of mean fluorescence intensity from rBMSCs was faster than L929, which indicated that more EVs played a role in the rBMSCs than L929 cells.

ERP-EVs promoted osteogenic differentiation of rBMSCs *in vitro*

After we determined the optimal combination ratio of ERP-EVs and certificated that ERP-EVs were selectively internalized by different types of cells. We co-cultured rBMSCs with 1:1 combined ERP-EVs for 7 days or 14 days. The alkaline phosphatase (ALP) activity of rBMSCs was increased in the ERP-EVs group, and ERP itself didn't promote the ALP activity of rBMSCs (Figure 4A). The ALP staining demonstrated the consistent result (Figure S3). Moving forward, the mRNA level of Type I collagen (Col-1) was significantly enhanced during the whole process. The mRNA level of Sp7 had an early enhancement on 7 days while Osteopontin (OPN) increased on 14 days (Figure 4B). Similarly, Col-1 and OPN protein expression in ERP-EVs increased significantly on 14 days (Figure 4D). However, the difference between Sp7 protein expression in the three group samples was not much obvious. Last, Alizarin Red S (ARS) staining assay indicated that the calcium nodule formation ability of

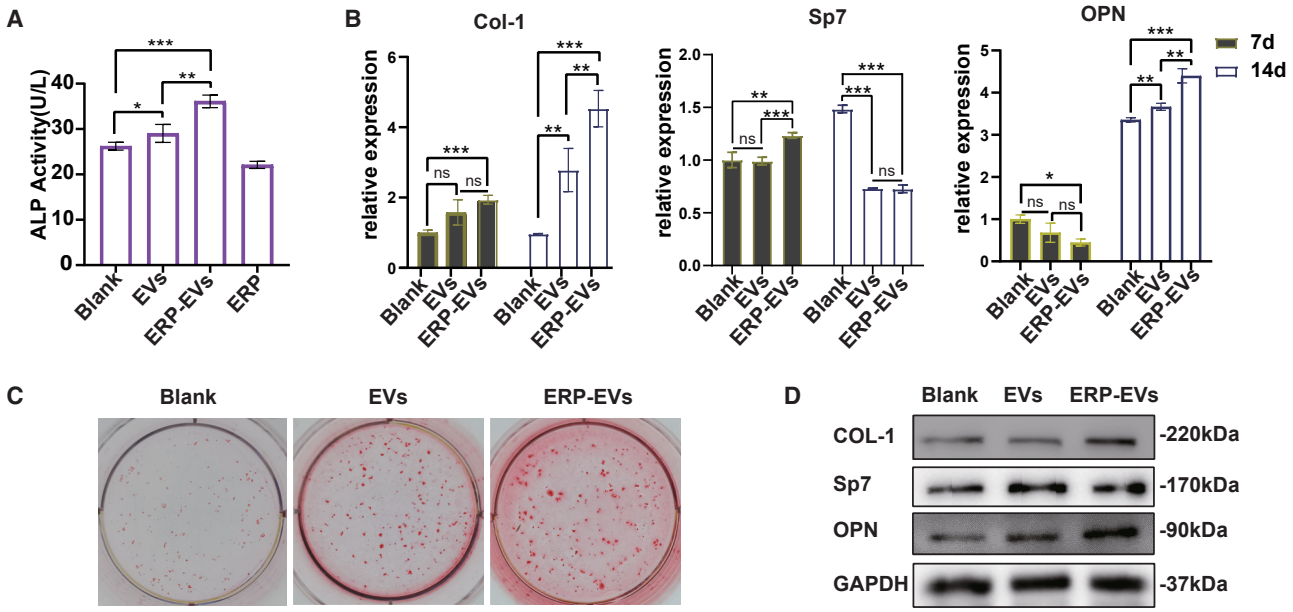

Figure 4. ERP-EVs promoted osteoblastic differentiation of rBMSCs

(A) Quantitation of ALP activity of rBMSCs co-cultured with EVs and ERP-EVs for 7 days.

(B) Real-time qPCR was used to analyze the relative mRNA expression level of bone-specific markers Col-1, Sp7, and OPN. Data are presented as mean ± SEM. Differences in expression between groups were calculated by one-way ANOVA. ($n = 3$, *$p < 0.05$, **$p < 0.01$, ***$p < 0.001$).

(C) The effect of EVs and ERP-EVs on calcium deposition of rBMSCs after co-culture for 21 days.

(D) Western blot analysis of bone-specific markers COL-1, Sp7, and OPN expressions.

the ERP-EVs sample was significantly enhanced (Figure 4C). Collectively, these data demonstrated that ERP-EVs enhanced osteogenic differentiation of rBMSCs *in vitro*.

ERP-EVs-nHA/CS-MS scaffold promoted osteogenic differentiation of rBMSCs *in vitro*

After we confirmed the osteogenic effects of ERP-EVs on rBMSCs, we wanted to determine whether it could be combined with the nHA/CS-MS scaffold, and if ERP-EVs-nHA/CS-MS scaffold could also promote osteogenic differentiation of rBMSCs *in vitro*. Firstly, the morphology of nHA/CS-MS (Figure S4A) and immunofluorescence assay to demonstrate the attachment of ERP-EVs on nHA/CS-MS (Figure S4B). The results revealed that microspheres with the diameter ranging from 250 μm to 500 μm presented the hierarchical nanofibrous structure. Additionally, PKH67-ERP-EVs (yellow arrows) successfully adhered to scaffolds. Then, rBMSCs were co-cultured with nHA/CS-MS and ERP-EVs-nHA/CS-MS microspheres for 24 h, the live/dead assay revealed that nHA/CS-MS and ERP-EVs-nHA/CS-MS microspheres displayed high cell viability during 24 h culture (Figure 5A), further verifying biocompatibility of the scaffolds. These data also indicated that ERP-EVs-nHA/CS-MS microspheres supported cell adhesion. To test the rate of releasing ERP-EVs for this loading scaffold, the cumulative release amount of ERP-EVs was measured by NTA after 0, 1, 2, 4, 24, and 48 h. The result indicated that the majority of ERP-EVs had released within the first 4 h (Figure 5B). Moreover, cell viability was measured after co-culture of rBMSCs with blank scaffold and loading scaffold at 24 h, indicating that both ERP-EVs loaded scaffold and blank scaffold significantly increased cell survival (Figure 5C). It was noted that ALP activity in ERP-EVs loaded scaffold samples were significantly increased compared with other samples. Together, the ERP-EVs-nHA/CS-MS scaffold had the characteristics of good biocompatibility that were beneficial for the osteogenic differentiation of rBMSCs *in vitro* (Figure 5D).

ERP-EVs-nHA/CS-MS scaffold promoted bone regeneration *in vivo*

The previous data demonstrated that the ERP-EVs-nHA/CS-MS scaffold could promote the osteogenesis of rBMSCs *in vitro*. Then calvarial bone defect SD rat model and nHA/CS-MS scaffold or ERP-EVs-nHA/CS-MS scaffold was planted in the defect area. We found that the new bone formation at ERP-EVs-nHA/CS-MS scaffold significantly promoted the new bone formation compared with the control group and the MS group (Figure 6A). Bone surface area/bone volume (BS/BV), bone mineral density (BMD), and trabecular number (Tb.N) in the ERP-EVs-MS sample group were significantly larger than those in the control group and MS scaffold group (Figure 6C). Hematoxylin-eosin staining (Figure S5) and Masson-trichrome staining (Figure 6C) showed new bone regeneration and collagen formation from the calvarial bone defect margins, and some new bones (black arrows in Figure S5) regenerated around unabsorbed ERP-EVs-MS scaffold (yellow arrows in Figure 6C). Additionally, the result of immunohistochemistry staining showed that OPN and SP7 expressed in ERP-EVs-nHA/CS-MS scaffolds *in vivo* (Figure S6), indicating the enhanced bone regeneration.

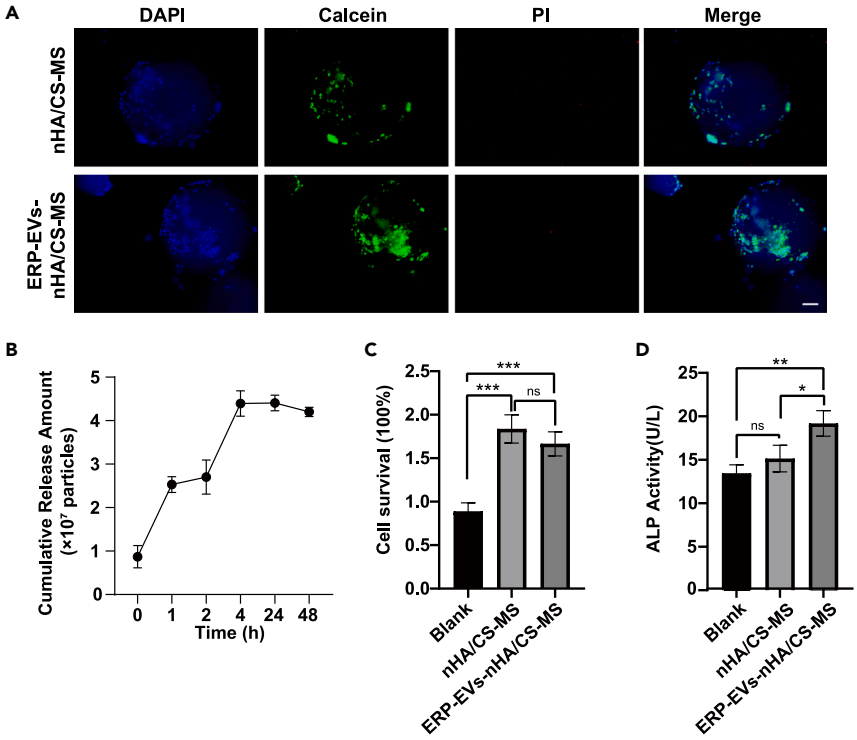

Figure 5. Biological characterization and osteogenic effect of ERP-EVs-nHA/CS-MS

(A) The adhesion of rBMSCs to nHA/CS-MS and ERP-EVs-nHA/CS-MS scaffolds via live/dead staining after co-culture with rBMSCs for 24 h. Scale bar, 100 μm.

(B) The cumulative release amount of ERP-EVs by nHA/CS-MS at different time points detected by NTA.

(C) CCK-8 was used to detect the effect of blank and loading scaffold on cell proliferation at 24 h.

(D) The ALP activity of rBMSCs co-cultured blank and loading scaffold for 7 days was quantitatively tested. Data are presented as mean ± SEM. Differences in expression between groups were calculated by one-way ANOVA. (n = 3, *p < 0.05, **p < 0.01, ***p < 0.001).

DISCUSSION

In this study, we demonstrated that ERP-EVs significantly enhanced rBMSCs uptake efficiency relative to un-modified bone-related cells due to esterase-response charge reversal. ERP-EVs significantly enhanced osteogenesis differentiation of rBMSCs *in vitro* and new bone formation in rat calvarial bone defect model *in vivo*.

Though it is reported that EVs derived from MSCs have the potential to promote tissue regeneration,[18,19] the great challenges for clinical application is restricted by the high cost and time-consuming operation for EV isolation. We noticed that the efficiency of recipient cells uptaking BMSCs-EVs was relatively low and strongly heterogeneous,[20,21] leading to a waste of EVs. This might be the reason why we need a huge amount of EVs.

We considered modifying BMSCs-EVs by reversing the charges of EVs with nanoparticles ERP to improve the uptake efficiency. ERP is a cationic polymer. Cationic polymers commonly combine negatively charged nucleic acid molecules by electrostatic force to form positively charged nanocomplexes. Like nucleic acid, EVs are negatively charged. When ERP and EVs formed ERP-EVs complex, positively charged ERP-EVs could be uptaken faster by host cells with negatively charged plasma membranes through electrostatic force. Similarly, Petro et al. used PEI-modified EVs to enhance the delivery of siRNA.[11] Kai Feng et al. utilized εPL-PEG-DSPE to reverse the surface charge of MSCs-derived EVs and demonstrated that PPD-sEVs significantly enhanced cartilage uptake and penetration as compared to MSC-sEVs. In our experiment, we found that ERP-EVs always showed a positive charge no matter what ratio we combined rBMSCs-EVs with ERP, indicating that ERP was an ideal modification carrier for EVs charge reverse.

In addition, the design of ERP in our experiment aimed to realize the differential release rate of EVs in bone tissues. Cells that were rich in esterase tended to "consume" more EVs that have been internalized into the cytoplasm. BMSCs, as a key cell for bone regeneration, were rich in esterase thus, we hoped that ERP-EVs "preferred" BMSCs, thereby promoting the osteogenesis differentiation of recipient cells effectively.

After one-step mixing EVs with ERP, the uptake efficiency was dramatically enhanced in rBMSCs. Meanwhile, the mean uptake efficiency by each recipient cell was also dramatically promoted, which was similar to the previous study.[21] The reason might be that ERP enhanced the electrostatic force between EVs and rBMSCs, which was beneficial for rBMSCs to quickly incorporate more EVs. However, we could not exclude that some ERP-EVs are attached to the recipient cells' surface. In other words, we could not quantify the exact amount of ERP-EVs uptaken into rBMSCs, which needs further investigation.

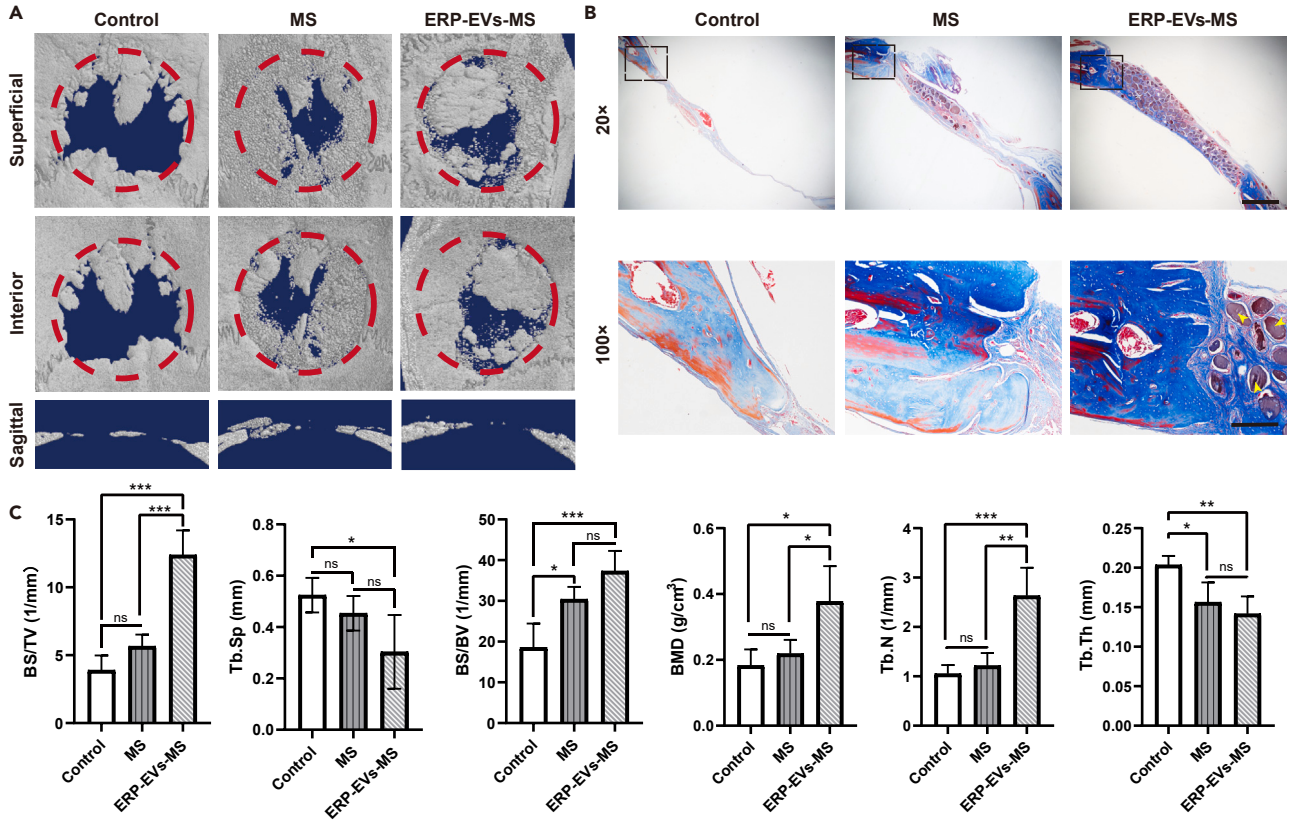

Figure 6. New bone regeneration *in vivo* after 8 weeks of implantation with ERP-EVs-nHA/CS-MS scaffold

(A) Two sides of the bone defect area and sagittal planes were captured. Original bone defect margins were marked with red dotted lines.

(B) Masson staining showed new bone regeneration and collagen formation respectively from the calvarial bone defect margins, new bone regenerated around the ERP-EVs-MS scaffold (yellow arrows). 20×, scale bar represents 1000 μm; 100×, scale bar represents 250 μm.

(C) Quantitative analysis of BS/TV, Tb. Sp, BS/BV, BMD, Tb.N and Tb.Th values of new bone formation at 8 weeks post-implantation. Data are presented as mean ± SEM. Differences in expression between groups were calculated by one-way ANOVA. ($n = 4$, $^{*}p < 0.05$, $^{**}p < 0.01$, $^{***}p < 0.001$).

We also hypothesized that rBMSCs cocultured with ERP-EVs could have more cell communication than those un-modified EVs. Active cell communication means more secreted EVs. We tested the number of EVs in the supernatant after coculture. However, the results showed that there was no significant difference between the ERP-EVs group and the EVs group (data not shown). One reason might be that the majority of EVs played a role in recipient cells themselves, another reason might be that it still needs assessment with longer time points.

Because of the fluidity of EVs, a biomaterial scaffold is necessary for EV delivery in bone regeneration. Some scholars used HA-based hydrogel, collagen sponge, β-TCP, PLGA, etc. as bone formation scaffolds in pre-clinical studies.[22] It is critical to increase the number of EVs attached to scaffolds and control the release rate of EVs after loading. EVs could be loaded on a scaffold by simply incubation. Li et al. immersed PLGA/pDA scaffold in adipose stem cells-derived EVs solution.[23] Zhang et al. blotted human MSCs onto β-TCP scaffold and left them still for incubation.[24] Meanwhile, some studies showed the limitations of integrating EVs into scaffolds by physical adsorption alone. The time for releasing EVs from scaffolds is not enough to support bone regeneration and repair for several weeks. Zhai et al. loaded EVs derived from human MSCs on the surface of 3D-printed titanium scaffolds and monitored them for 50 h using EV release spectroscopy. However, 50% of the loaded EVs are released only after 3 h, showing the initial burst release stage.[25]

HE and Masson staining were utilized for new bone formation assessment. The bone defect repair we observed was not solely the result of more uptakes of ERP-EVs, nHA/CS-MS scaffold was also involved in the mineralization of the defect area. The new bone was generated from the margin of calvarial bone defect areas in all three experimental groups. Some new bone was generated around the remaining nHA/CS-MS, indicating that the ERP-EVs-loaded scaffold enhanced new bone regeneration. Besides, nHA/CS-MS promoted the cell adhesion and proliferation of rBMSCs *in vitro* (Figures 5A and 5C). Some studies focusing on HA/CS scaffold also indicated significant effects for proliferation, migration, and osteogenic differentiation of MSCs.[26,27] As for the degradation profile of the scaffold, some studies conducted the *in vitro* degradation evaluation, microspheres were immersed in lysozymes solution and incubated at 37°C with shaking. Images indicated that almost no degradation process for more than 5 weeks of incubation.[28,29] However, the scaffolds were degradable *in vivo*. In our study, some partly degraded nHA/CS-MS scaffolds remained in bone defect areas after 8 weeks of implantation with the diameter decreased by

approximately 200 μm (Figure S5). The longer time point should be recorded in further research to assess the degradation rate of the nHA/CS-MS scaffold.

In conclusion, our experiment indicated that ERP promoted the uptake efficiency of recipient cells, thereby enhancing the rBMSCs osteogenesis differentiation *in vitro*. Meanwhile, the ERP-EVs-loaded nHA/CS-MS scaffold significantly improved new bone formation *in vivo*.

Limitations of study

In this study, we assumed that ERP-EVs could be efficiently uptake by recipient cells with high esterase. However, the esterase-response characteristics of other bone-related cells should be taken into consideration due to the complicated and changeable bone microenvironments *in vivo*. Therefore, future work is warranted to break through these limitations.

RESOURCE AVAILABILITY

Lead contact

Further information and requests for resources and reagents should be directed to and will be fulfilled by the lead contact, Jianguang Xu (xujianguang@ahmu.edu.cn).

Materials availability

This study did not generate new unique reagents.

Data and code availability

- All data reported in this paper will be shared by the lead contact upon request.
- This paper does not report original code.
- Any additional information required to reanalyze the data reported in this paper is available from the lead contact upon request.

ACKNOWLEDGMENTS

This work was supported by the Anhui Provincial Health Commission project under grant AHWJ2022b002; and the Natural Science Foundation of Anhui Institute of Translational Medicine under grant 2022zhyx-C87.

AUTHOR CONTRIBUTIONS

Y.C. wrote the manuscript. Y.C. and B.L. designed and performed most of the experiments. M.C., N.E., and W.H. contributed to animal study. H.Z., N.Q., and H.Z. revised the manuscript. J.X. supervised the project.

DECLARATION OF INTERESTS

The authors declare no competing interests.

STAR★METHODS

Detailed methods are provided in the online version of this paper and include the following:

- KEY RESOURCES TABLE
- EXPERIMENTAL MODEL AND STUDY PARTICIPANT DETAILS
  - Cell culture
  - Animals
- METHOD DETAILS
  - Isolation and characterization of rBMSCs-derived EVs
  - EV labeling and uptake efficiency of recipient cells
  - EVs modification by ERP
  - Fluorescein diacetate measuring cellular esterase activity
  - Cell proliferation assay
  - RNA extraction, reverse transcription, and quantitative PCR
  - Western Blot analysis
  - Alkaline phosphatase quantitative assay and alizarin red S staining
  - Preparation of ERP-EVs nHA/CS-MS scaffold
  - Live/dead assay for cell viability on scaffolds
  - The release rate of ERP-EVs from nHA/CS-MS scaffold
  - Scaffold implantation *in vivo*
  - Micro-CT analysis
  - Histological analysis
- QUANTIFICATIONS AND STATISTICAL ANALYSIS

SUPPLEMENTAL INFORMATION

Supplemental information can be found online at https://doi.org/10.1016/j.isci.2024.110801.

Received: March 26, 2024
Revised: June 28, 2024
Accepted: August 20, 2024
Published: August 23, 2024

REFERENCES

1. Palti, A., and Hoch, T. (2002). A concept for the treatment of various dental bone defects. Implant Dent. *11*, 73–78. https://doi.org/10.1097/00008505-200201000-00017.
2. Schmitt, C.M., Doering, H., Schmidt, T., Lutz, R., Neukam, F.W., and Schlegel, K.A. (2013). Histological results after maxillary sinus augmentation with Straumann® BoneCeramic, Bio-Oss®, Puros®, and autologous bone. A randomized controlled clinical trial. Clin. Oral Implants Res. *24*, 576–585. https://doi.org/10.1111/j.1600-0501.2012.02431.x.
3. Zhou, T., Yuan, Z., Weng, J., Pei, D., Du, X., He, C., and Lai, P. (2021). Challenges and advances in clinical applications of mesenchymal stromal cells. J. Hematol. Oncol. *14*, 24. https://doi.org/10.1186/s13045-021-01037-x.
4. Infante, A., Alcorta-Sevillano, N., Macías, I., and Rodríguez, C.I. (2022). Educating EVs to Improve Bone Regeneration: Getting Closer to the Clinic. Int. J. Mol. Sci. *23*, 1865. https://doi.org/10.3390/ijms23031865.
5. Kalluri, R., and LeBleu, V.S. (2020). The biology, function, and biomedical applications of exosomes. Science (New York, N.Y.) *367*, eaau6977. https://doi.org/10.1126/science.aau6977.
6. Kim, H.J., Kim, G., Lee, J., Lee, Y., and Kim, J.H. (2022). Secretome of Stem Cells: Roles of Extracellular Vesicles in Diseases, Stemness, Differentiation, and Reprogramming. Tissue Eng. Regen. Med. *19*, 19–33. https://doi.org/10.1007/s13770-021-00406-4.
7. Kang, M., Lee, C.S., and Lee, M. (2021). Bioactive Scaffolds Integrated with Liposomal or Extracellular Vesicles for Bone Regeneration. Bioengineering *8*, 137. https://doi.org/10.3390/bioengineering8100137.
8. Sato, Y.T., Umezaki, K., Sawada, S., Mukai, S.A., Sasaki, Y., Harada, N., Shiku, H., and Akiyoshi, K. (2016). Engineering hybrid exosomes by membrane fusion with liposomes. Sci. Rep. *6*, 21933. https://doi.org/10.1038/srep21933.
9. Tian, T., Zhang, H.X., He, C.P., Fan, S., Zhu, Y.L., Qi, C., Huang, N.P., Xiao, Z.D., Lu, Z.H., Tannous, B.A., and Gao, J. (2018). Surface functionalized exosomes as targeted drug delivery vehicles for cerebral ischemia therapy. Biomaterials *150*, 137–149. https://doi.org/10.1016/j.biomaterials.2017.10.012.
10. Zha, Y., Lin, T., Li, Y., Zhang, X., Wang, Z., Li, Z., Ye, Y., Wang, B., Zhang, S., and Wang, J. (2020). Exosome-mimetics as an engineered gene-activated matrix induces in-situ vascularized osteogenesis. Biomaterials *247*, 119985. https://doi.org/10.1016/j.biomaterials.2020.119985.
11. Zhupanyn, P., Ewe, A., Büch, T., Malek, A., Rademacher, P., Müller, C., Reinert, A., Jaimes, Y., and Aigner, A. (2020). Extracellular vesicle (ECV)-modified polyethylenimine (PEI) complexes for enhanced siRNA delivery in vitro and in vivo. J. Contr. Release *319*, 63–76. https://doi.org/10.1016/j.jconrel.2019.12.032.
12. Lockridge O, Q.D., and Radić, Z. (2018). Esterases. Biotransformations *10–15*, 277–307. https://doi.org/10.1016/B978-0-12-801238-3.01970-X.
13. Qiu, N., Liu, X., Zhong, Y., Zhou, Z., Piao, Y., Miao, L., Zhang, Q., Tang, J., Huang, L., and Shen, Y. (2016). Esterase-Activated Charge-Reversal Polymer for Fibroblast-Exempt Cancer Gene Therapy. Adv. Mater. *28*, 10613–10622. https://doi.org/10.1002/adma.201603095.
14. Evans, J.D. (1952). Acetoacetate and esterase activity in normal rabbit bone marrow in vitro. Am. J. Physiol. *171*, 48–54. https://doi.org/10.1152/ajplegacy.1952.171.1.48.
15. Farnes, P., and Barker, B.E. (1964). CYTOCHEMICAL STUDIES OF HUMAN BONE MARROW FIBROBLAST-LIKE CELLS. II. ESTERASE AND ACID PHOSPHATASE. Am. J. Pathol. *44*, 481–489.
16. Lau, W.M., Ng, K.W., Sakenyte, K., and Heard, C.M. (2012). Distribution of esterase activity in porcine ear skin, and the effects of freezing and heat separation. Int. J. Pharm. *433*, 10–15. https://doi.org/10.1016/j.ijpharm.2012.04.079.
17. Ruyuan Ding, Y.L., Cheng, D., Yang, G., Wu, W., Du, H., Jin, X., Chen, Y., Wang, Y., HENG, B.C., Yang, Q., and Jianguang, X.U. (2022). A novel gene-activated matrix composed of PEI/plasmid-BMP2 complexes and hydroxyapatite/chitosan-microspheres promotes bone regeneration. Nano Res. *15*, 6348–6360. https://doi.org/10.1007/s12274-022-4292-8.
18. Song, Y., You, Y., Xu, X., Lu, J., Huang, X., Zhang, J., Zhu, L., Hu, J., Wu, X., Xu, X., et al. (2023). Adipose-Derived Mesenchymal Stem Cell-Derived Exosomes Biopotentiated Extracellular Matrix Hydrogels Accelerate Diabetic Wound Healing and Skin Regeneration. Adv. Sci. *10*, e2304023. https://doi.org/10.1002/advs.202304023.
19. Kiang, J.G. (2021). Mesenchymal stem cells and exosomes in tissue regeneration and remodeling: characterization and therapy. In Tissue Barriers in Disease, Injury and Regeneration (Elsevier), pp. 159–185. https://doi.org/10.1016/B978-0-12-818561-2.00005-9.
20. Deng, C., Dong, K., Liu, Y., Chen, K., Min, C., Cao, Z., Wu, P., Luo, G., Cheng, G., Qing, L., and Tang, J. (2023). Hypoxic mesenchymal stem cell-derived exosomes promote the survival of skin flaps after ischaemia-reperfusion injury via mTOR/ULK1/FUNDC1 pathways. J. Nanobiotechnol. *21*, 340. https://doi.org/10.1186/s12951-023-02098-5.
21. Feng, K., Xie, X., Yuan, J., Gong, L., Zhu, Z., Zhang, J., Li, H., Yang, Y., and Wang, Y. (2021). Reversing the surface charge of MSC-derived small extracellular vesicles by epsilonPL-PEG-DSPE for enhanced osteoarthritis treatment. J. Extracell. Vesicles *10*, e12160. https://doi.org/10.1002/jev2.12160.
22. Tan, S.H.S., Wong, J.R.Y., Sim, S.J.Y., Tjio, C.K.E., Wong, K.L., Chew, J.R.J., Hui, J.H.P., and Toh, W.S. (2020). Mesenchymal stem cell exosomes in bone regenerative strategies-a systematic review of preclinical studies. Mater. Today. Bio *7*, 100067. https://doi.org/10.1016/j.mtbio.2020.100067.
23. Li, W., Liu, Y., Zhang, P., Tang, Y., Zhou, M., Jiang, W., Zhang, X., Wu, G., and Zhou, Y. (2018). Tissue-Engineered Bone Immobilized with Human Adipose Stem Cells-Derived Exosomes Promotes Bone Regeneration. ACS Appl. Mater. Interfaces *10*, 5240–5254. https://doi.org/10.1021/acsami.7b17620.
24. Zhang, J., Liu, X., Li, H., Chen, C., Hu, B., Niu, X., Li, Q., Zhao, B., Xie, Z., and Wang, Y. (2016). Exosomes/tricalcium phosphate combination scaffolds can enhance bone regeneration by activating the PI3K/Akt signaling pathway. Stem Cell Res. Ther. *7*, 136. https://doi.org/10.1186/s13287-016-0391-3.
25. Zhai, M., Zhu, Y., Yang, M., and Mao, C. (2020). Human Mesenchymal Stem Cell Derived Exosomes Enhance Cell-Free Bone Regeneration by Altering Their miRNAs Profiles. Adv. Sci. *7*, 2001334. https://doi.org/10.1002/advs.202001334.
26. Jamalpoor, Z., Taromi, N., Soleimani, M., Koudehi, M.F., and Asgari, A. (2019). In vitro interaction of human Wharton's jelly mesenchymal stem cells with biomimetic 3D scaffold. J. Biomed. Mater. Res. *107*, 1166–1175. https://doi.org/10.1002/jbm.a.36608.
27. Mohd Zaffarin, A.S., Ng, S.F., Ng, M.H., Hassan, H., and Alias, E. (2021). Nano-Hydroxyapatite as a Delivery System for Promoting Bone Regeneration In Vivo: A Systematic Review. Nanomaterials *11*, 2569. https://doi.org/10.3390/nano11102569.
28. Cheng, D., Ding, R., Jin, X., Lu, Y., Bao, W., Zhao, Y., Chen, S., Shen, C., Yang, Q., and Wang, Y. (2023). Strontium Ion-Functionalized Nano-Hydroxyapatite/Chitosan Composite Microspheres Promote Osteogenesis and Angiogenesis for Bone Regeneration. ACS Appl. Mater. Interfaces *15*, 19951–19965. https://doi.org/10.1021/acsami.3c00655.
29. Lu, Y., Wang, Z.-Y., Xiao, J., Zhao, Z., Liao, X., Gao, H.-L., and Zou, D. (2024). Multifunctional chitosan-based nanocomposite microgels for reconstructing osteochondral defects. Mater. Des. *239*, 112821. https://doi.org/10.1016/j.matdes.2024.112821.
30. Schneider, C.A., Rasband, W.S., and Eliceiri, K.W. (2012). NIH Image to ImageJ: 25 years of image analysis. Nat. Methods *9*, 671–675. https://doi.org/10.1038/nmeth.2089.
31. Spicer, P.P., Kretlow, J.D., Young, S., Jansen, J.A., Kasper, F.K., and Mikos, A.G. (2012). Evaluation of bone regeneration using the rat critical size calvarial defect. Nat. Protoc. *7*, 1918–1929. https://doi.org/10.1038/nprot.2012.113.

STAR★METHODS

KEY RESOURCES TABLE

REAGENT or RESOURCE	SOURCE	IDENTIFIER
Antibodies		
Anti-Sp7/Osterix antibody [EPR21034]	Abcam	ab209484; RRID:AB_2892207
Anti-Collagen I antibody [EPR22209-75]	Abcam	ab255809; RRID:AB_3097801
Anti-Osteopontin antibody [RM1018]	Abcam	ab283656; RRID:AB_2894861
GAPDH (14C10) Rabbit mAb #2118	Cell Signaling Technology	Cat#2118S; RRID:AB_561053
Chemicals, peptides, and recombinant proteins		
PBS (no calcium, no magnesium)	VivaCell	Cat#C3580-0500
Fetal bovine serum (FBS)	VivaCell	Cat#C04001-500
Exosome depleted Fetal Bovine Serum	VivaCell	Cat#C38010050
α-MEM	Gibco	Cat#C12571500BT
Penicillin-Streptomycin Solution, 100X	Beyotime	Cat#C0222
Fluorescein diacetate	Yeasen	Cat#40720ES03
RIPA lysis buffer	Beyotime	Cat#P0013
Alizarin Red S	Sigma-Aldrich	A5533
Critical commercial assays		
PKH67 Green Fluorescent Cell Linker Kit	Sigma-Aldrich	PKH67GL
Cell Counting Kit-8	Dojindo	Cat#CK04
RNA-Quick Purification Kit	ES Science	Cat#RN001
Prime Script RT reagent Kit	TaKaRa	Cat#RR037A
SYBR Premix Ex Taq	TaKaRa	Cat#RR420A
BCIP/NBT Alkaline Phosphatase Color Development Kit	Beyotime	Cat#C3206
Calcein/PI cell viability and cytotoxicity kit	Beyotime	Cat#C2015S
Experimental models: Cell lines		
SD Rat: Passage 2–6 BMSCs	This paper	N/A
Mouse: L-929	ATCC	CCL-1
Oligonucleotides		
Primer: GAPDH Forward: ACAGCAACAGGGTGGTGGAC	This paper	N/A
Primer: GAPDH Reverse: TTTGAGGGTGCAGCGAACTT	This paper	N/A
Primer: OPN Forward: GACGATGATGACGACGATGAC	This paper	N/A
Primer: OPN Reverse: GTGTGCTGGCAGTGAAGGACTC	This paper	N/A
Primer: COL1 Forward: CAGCGGAGGAGGCTATGACTTT	This paper	N/A
Primer: COL1 Reverse: GGCGAGATGGCTTATTCGTTTT	This paper	N/A
Primer: Sp7 Forward: CAGCCTGCAGCAAGTTTGG	This paper	N/A
Primer: Sp7 Reverse: TTTTCCCAGGGCTGTTGAGT	This paper	N/A

(*Continued on next page*)

Continued

REAGENT or RESOURCE	SOURCE	IDENTIFIER
Software and algorithms		
ImageJ	Schneider et al.[30]	https://imagej.nih.gov/ij/
CTVox	Bruker	https://www.bruker.com/en/products-and-solutions

EXPERIMENTAL MODEL AND STUDY PARTICIPANT DETAILS

Cell culture

Rat BMSCs were derived in culture from Sprague-Dawley (SD) rats' bone marrow. Briefly, 3-week-old male SD rats were sacrificed by decapitation. The bone marrow was washed 3–4 times from the femur and tibia with 1×PBS (VivaCell, catalog no. C3580-0500). After centrifugation at 900 rpm for 5 min, the bone marrow was suspended using α-MEM culture medium (Gibco, catalog no. C12571500BT), supplemented with 20% (v/v) FBS (VivaCell, catalog no. C04001-500) and 1% penicillin/streptomycin (Beyotime, catalog no. C0222). Cells were allowed to attach for 3–4 days after the non-adherent cell population was removed and the culture medium was replaced with fresh culture α-MEM culture medium supplemented with 10% (v/v) FBS and 1% penicillin/streptomycin. The culture medium was changed twice a week.

NCTC clone 929 cell line (L929) was kindly provided as a gift by Dr. Jialong Chen (Department of Biomaterials, Anhui Province Key Laboratory of Oral Diseases Research). L929 was cultured with MEM (Procell, catalog no. PM150410) medium supplemented with 5% (v/v) FBS and 1% penicillin/streptomycin. The culture medium was changed every two days. All cells were cultured in a humidified atmosphere with 5% CO_2 at 37°C.

Animals

Twelve male SD rats (250 g) aged 8 weeks old were used in this study and were randomly assigned to three experimental groups. All animals were housed on a 12 h light/dark cycle at 23°C with free access to food and water. The surgical procedures were ethically approved by the Animal Ethics Committee of Anhui Medical University (LLSC20231873).

METHOD DETAILS

Isolation and characterization of rBMSCs-derived EVs

Briefly, after 2 or 3 passages, rBMSCs were incubated in α-MEM culture medium, supplemented with 10% (v/v) EV-deleted FBS (VivaCell, catalog no. C38010050) and 1% penicillin/streptomycin. The supernatant was harvested when passaging cells or changing medium. The harvested supernatant was centrifuged at 2000 g, 4°C for 10 min, and 10000 g, 4°C for 30 min to remove cell debris. Then the pretreated supernatant was ultracentrifuged by Optimal XE-100 ultracentrifuge (Beckman) at 120000 g, 4°C for 70 min to remove the supernatant. Finally, the EV pellet was suspended with abundant PBS and was ultracentrifuged again to gain pure EVs. The EVs were suspended with 50 μL PBS for further storage and experiments.

EVs were quantified using a nanoparticle tracking analyzer (NTA; Malvern, Nanosight 300). Briefly, the EV suspension was diluted 500 times with PBS for texting. Approximately 2×10^8 rBMSCs could generate around 2×10^{11} EV. For *in vitro* study concerning osteogenic differentiation, EV pellets were resuspended in fresh culture medium at the concentration of 1×10^6 particles/mL.

TEM (Thermo Scientific, Talos, L120C G2) was used to observe and acquire images of the morphology of EVs. EV pellets were resuspended in 1% glutaraldehyde for 30 min. Samples were dripped on Formvar-coated copper grids and incubated for 20 min. After washing, samples were negatively stained with 2.5% uranyl acetate for 5 min. Last, the specific biomarker CD9 was measured by Western Blot using the protocol detailed in the 'western blot analysis' section.

EV labeling and uptake efficiency of recipient cells

EVs were labeled with a PKH67 Green Fluorescent Cell Linker Kit (Sigma) for visualization. According to the manufacturer's instruction, 2 μL of PKH67 dye solution was added into 0.5 mL Diluent C whereas EVs were resuspended into another 0.5 mL Diluent C. Afterward, mixed and incubated in the dark for 2 min. 1% BSA was added to terminate the staining process. Finally, the solution was suspended with abundant PBS and ultracentrifuged at 120000×g, 4°C for 70 min to gain PKH67 labeled EVs. 3×10^4 BMSCs per well were seeded into 24 well-plate. Then, EV pellets were resuspended in fresh culture medium at the concentration of 1.5×10^8 particles/mL and were co-cultured with BMSCs for 4h.

The uptake efficiency of recipient cells was observed by laser scanning confocal microscope (Zeiss, LSM800), and was quantified by ImageJ for their mean fluorescence intensity.

EVs modification by ERP

ERP was a gift given by Dr. Nasha Qiu (Hangzhou First People's Hospital). EVs were simply mixed with ERP in 0.5 mL PBS with different ratios (1:0, 5:1, 2:1, 1:1), and incubated for 15 min at room temperature before testing. The size of ERP and the zeta potential of ERP and ERP-EVs were measured at 25°C using dynamic light scattering (DLS; Malvern, ZSU3100).

Fluorescein diacetate measuring cellular esterase activity

The esterase activity L929 and rBMSCs were incubated using 5 μg/mL FDA (Yeasen, catalog no. 40720ES03) working solution for 30 min. FITC fluorescence intensity at 530 nm excited at 480 nm was measured for each cell using a multifunctional microplate detector (TECAN, Spark) every 30 min for 2 h. Fluorescence intensity values at different time points for both cells were normalized by cell number per well.

Cell proliferation assay

A Cell Counting Kit-8 assay (CCK-8; Dojindo, catalog no. CK04) was performed to assess cytotoxicity or cell proliferation. Briefly, rBMSCs were seeded onto 96-well plates at the cell density of 5×10^3 cells per well and cultured at 37°C, 5% CO_2 in EV-free media supplemented with 1×10^6 particles/mL of EVs or the same concentration of EVs combined with ERP in 1:1 ratio. Cells treated with an equal volume of PBS were served as controls, and a group without cells was served as the blank. On day 1 and day 2, CCK-8 solution (10 μL per well) was added to rBMSCs and subsequently incubated at 37°C for 1 h. The absorbance was measured at 450 nm using a microplate reader. The optical density (OD) values represented the survival/proliferation of rBMSCs.

RNA extraction, reverse transcription, and quantitative PCR

To assess the mRNA level of rBMSCs after coculture with EVs or ERP-EVs at 7 days and 14 days, RNA was isolated from cells using an RNAQuick Purification Kit (ES Science, catalog no. RN001) according to the manufacturer's instruction. cDNA was synthesized using the Prime Script RT reagent Kit (TaKaRa, catalog no. RR037A). Quantitative real-time PCR was proceeded using LightCycler 96 System (Roche) and SYBR Premix Ex Taq (TaKaRa, catalog no. RR420A). Results were presented as $2^{-\Delta\Delta Ct}$ values normalized to the expression of OPN, Col-1, Sp7. Means and standard deviations were calculated.

Western Blot analysis

Cocultured rBMSCs on day 14 were lysed in RIPA lysis buffer (Beyotime, catalog no. P0013). The protein samples were separated by 10% SDS-PAGE, transferred to polyvinylidene difluoride membranes, which were blocked with 5% non-fat milk, washed with tris-buffered saline containing 0.1% Tween 20 (TBST), incubated overnight with primary antibodies (key resources table) at 4°C, and then incubated with Goat Anti-Rabbit IgG (ZSGB-Bio, catalog no. ZB-2301) at room temperature for 1 h. After washing with TBST, protein bands were detected using a chemiluminescence system (Vilber, Fusion FX).

Alkaline phosphatase quantitative assay and alizarin red S staining

After 7 days and 21 days cocultured with EVs and ERP-EVs, rBMSCs were harvested to assess the ALP activity using the BCIP/NBT kit (Beyotime, catalog no. C3206) and the formation of mineralized nodules using alizarin red S (Sigma, catalog no. A5533), respectively. As for ALP quantitative assay, rBMSCs were lysed by RIPA on ice for 30 min and were measured by a BCA protein assay kit (Beyotime, catalog no. P0010). Afterward, samples were treated according to the manufacturer's instruction for BCIP/NBT kit. A multifunctional microplate detector (TECAN, Spark) was used to measure the optical density. As for alizarin red S staining, the powder was diluted with ddH_2O, and the pH was adjusted to 8.3. Alizarin red S solution was then incubated with cells for 1 h in the dark. The deposition of calcium nodules in each group was observed under an inverted phase contrast microscope (Nikon, ECLIPSE Ts2).

Preparation of ERP-EVs nHA/CS-MS scaffold

nHA/CS-MS scaffold was originally stored in absolute ethyl alcohol. Before combination with ERP-EVs, MS scaffold was stewed overnight to layer the scaffold and solution. Then, the supernatant was discarded, and MS scaffold was washed with PBS twice by centrifugation at 5000 rpm for 15 min. 1×10^9 particles/mL of ERP-EVs were mixed with nHA/CS-MS scaffold and incubated overnight at 4°C. The supernatant was discarded to achieve the ERP-EVs-nHA/CS-MS scaffold.

Live/dead assay for cell viability on scaffolds

The viability of rBMSCs on nHA/CS-MS and ERP-EVs-nHA/CS-MS scaffolds was investigated via Calcein/PI cell viability kit (Beyotime, catalog no. C2015S). nHA/CS-MS and ERP-EVs-nHA/CS-MS scaffolds were co-cultured with rBMSCs for 24h. According to the manufacturer's instructions, the scaffolds were washed with PBS and incubated with Calcein/PI working buffer for 30 min in the dark. The scaffolds were observed by laser scanning confocal microscope (Zeiss, LSM800).

The release rate of ERP-EVs from nHA/CS-MS scaffold

500 μL PBS was added into 500 μL ERP-EVs-nHA/CS-MS scaffold to incubate for 0, 1, 2, 4, 24, 48h. At different time points, 500 μL solution was extracted to assess the particle number of ERP-EVs. The formula for calculating the cumulative absolute release number of ERP-EVs at each time point is as follows. (N: Cumulative number of particles released, unit "particles"; C: Particle concentration, unit "particle/mL").

$$N_{1st\ time\ point} = C_{1st}$$

$$N_{2nd\ time\ point} = 1/2\ C_{1st} + C_{2nd}$$

$$N_{3rd\ time\ point} = C_{3rd} + 1/2\ C_{2nd} + 1/2\ C_{1st}$$

$$N_{4th\ time\ point} = C_{4th} + 1/2\ C_{3rd} + 1/2\ C_{2nd} + 1/2\ C_{1st}$$

Scaffold implantation *in vivo*

Twelve male SD rats (250 g) aged 8 weeks old were used *in vivo* study and randomly assigned to three groups ($n = 4$): i) sham group; ii) blank scaffold group, and iii) ERP-EVs loaded scaffold group. The surgical procedures for calvarial bone defects were followed by the protocol.[31] Briefly, the animals were anesthetized by an intraperitoneal injection of pentobarbital. An 8 mm calvarial bone defect was created using an electric trephine cooled with 0.9% saline solution to ensure that the dura mater remained uninjured. The defects were filled with nHA/CS-MS scaffold and ERP-EVs-loaded nHA/CS-MS scaffold, respectively. For *in vivo* experiments, the total quantity of ERP-EVs loaded on the scaffold was approximately 1×10^{11} per rat. The animals were sacrificed by decapitation after 8 weeks, and then the craniums of rats were harvested for further experiments.

Micro-CT analysis

The harvested samples were scanned using a micro-CT scanner (Bruker, Skyscan 1176). The scanning energy was 65 kV/385 mA, and the voxel size was 9 μm. The Micro-CT 3D visualization software (CTVox) was used to obtain 2D reconstructed images. Bone surface area/bone volume (BS/BV), bone surface area/total volume (BS/TV), and trabecular spacing (Tb. Sp) were measured by an auxiliary software (Volume Graphics, VGSTUDIO MAX 3.0).

Histological analysis

The harvested samples were sequentially fixed with 4% paraformaldehyde for 48 h, decalcified with EDTA for 2 months and embedded with paraffin. Afterward, H&E and Masson staining were performed to evaluate the new bone tissue. The microscope (Nikon, ECLIPSE LV100POL) was used for image capture.

QUANTIFICATIONS AND STATISTICAL ANALYSIS

The data are expressed as the means ± the standard deviations, and statistically significant differences between datasets were evaluated with Student's t test, One-Way ANOVA, and two-Way ANOVA using GraphPad Prism 8. The threshold for statistical significance was set at $p < 0.05$. (*, $p < 0.05$; **, $p < 0.01$; ***, $p < 0.001$).